applied optics

# Performance evaluation of hybrid DPSK-MPPM techniques in long-haul optical transmission

Abdulaziz E. El-Fiqi,[1,2,6,*] Ahmed E. Morra,[2,4] Salem F. Hegazy,[3,4] Hossam M. H. Shalaby,[1,5] Kazutoshi Kato,[6] and Salah S. A. Obayya[4]

[1]Electronics and Communications Engineering Department, Egypt-Japan University of Science and Technology (E-JUST), Alexandria 21934, Egypt
[2]Electronics and Electrical Communications Engineering Department, Faculty of Electronic Engineering, Menoufia University, Menouf 32952, Egypt
[3]National Institute of Laser Enhanced Sciences, Cairo University, Giza 12613, Egypt
[4]Center for Photonics and Smart Materials, Zewail City of Science and Technology, Giza 12588, Egypt
[5]Electrical Engineering Department, Faculty of Engineering, Alexandria University, Alexandria 21544, Egypt
[6]Graduate School of Information Science and Electrical Engineering, Kyushu University, Fukuoka 819-0395, Japan
*Corresponding author: abdulaziz.elfiqi@ejust.edu.eg

Received 8 March 2016; revised 5 June 2016; accepted 16 June 2016; posted 17 June 2016 (Doc. ID 260437); published 14 July 2016

**In this paper, we evaluate the performance of hybrid differential phase shift keying-multipulse pulse position modulation (DPSK-MPPM) techniques in long-haul nonlinear-dispersive optical fiber transmission. An expression for the nonlinear interference variance is obtained analytically using the Gaussian noise (GN) model. We derive upper-bound expressions that take into account the fiber nonlinearity impact on the DPSK-MPPM system's performance for both bit- and symbol-error rates (BER and SER). The tightness of the BER's upper bound is verified using Monte Carlo simulation. The numerical analysis is carried out based on the proposed setup supplemented by a realistic simulation scenario for the DPSK-MPPM long-haul optical transmission system. Our results reveal that while the hybrid DPSK-MPPM technique outperforms both traditional DPSK and MPPM techniques under amplified spontaneous emission (ASE) noise (linear limit), it is less robust when fiber nonlinearity is considered. However, under the impact of low nonlinearity, the performance of a hybrid technique still surpasses the traditional ones. We also discuss the effect of some wavelength-division multiplexing (WDM) parameters on optimal system performance. The nonlinear interference penalties on the maximum reachable distances by both hybrid and traditional modulation systems are then investigated at a forward-error correction (FEC) requirement (BER = $10^{-3}$). In particular, at an average launch power of −8 dBm, the hybrid DQPSK-MPPM system with a total frame length of eight time slots including two signal time slots outreaches a traditional DQPSK system by 950 km.** 

***OCIS codes:*** (060.0060) Fiber optics and optical communications; (060.4080) Modulation; (060.4370) Nonlinear optics, fibers.

http://dx.doi.org/10.1364/AO.55.005614

## 1. INTRODUCTION

Hybrid modulation techniques improve the poor power efficiency of high-order modulation techniques, which represent a window for avoiding the optical capacity crunch in single-mode fibers (SMFs) [1]. In fact, these hybrid techniques can be used to increase the receiver sensitivity at a given bit-error rate (BER) [2]. Recently, several hybrid modulation techniques have been investigated for long-haul optical transmission [2–4]. For instance, Liu and co-workers demonstrated the transmission of a 6.23 Gbit/s PQ-4PPM (polarized multiplexed-quadrature phase shift keying in combination with 4-ary pulse position modulation) signal over a 370 km unrepeated ultra-large-area-fiber span with a total loss budget of 71.7 dB [2,3]. Furthermore, Sjödin *et al.* carried out the first experimental realization of hybrid polarized multiplexed-2PPM-quadrature phase shift keying (PM-2PPM-QPSK) modulation over a long-haul transmission distance up to 13,000 km with a data rate of 42.8 Gbit/s [4].

To the best of our knowledge, the analytical evaluation of the performance of hybrid modulation techniques in long-haul nonlinear-dispersive optical channels has not been addressed yet. In [5], we introduced a hybrid differential PSK-multipulse pulse position modulation (DPSK-MPPM) technique that is based on spectrally efficient direct-detection differential binary/quadrature PSK (DD-DBPSK/DD-DQPSK) techniques along with an energy-efficient MPPM technique. The DPSK-MPPM frame has time duration $T$ and is composed of $M$ successive time slots, each with time-slot duration $\tau$. These $M$ time slots are composed of $n$ signal (occupied) slots and $(M - n)$ nonsignal (vacant) slots, where the positions of the signal time slots are specified by the transmitted data bits. In addition, the MPPM signal time slots are DPSK modulated.

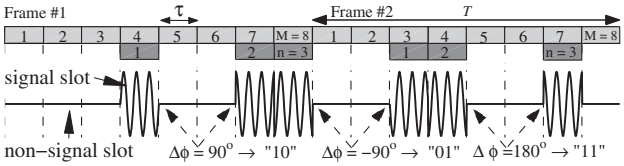


**Fig. 1.** Time domain sketch of two transmitted DQPSK-MPPM frames with ($M = 8$ and $n = 3$); $\Delta\phi$, phase difference between two successive DPSK symbols (signal slots); $T$, frame length; $\tau$, time-slot duration; $M$, total successive time slots per frame; $n$, number of the signal (occupied) time slots per frame.

These frame specifications are shown in Fig. 1 for a transmitted DQPSK-MPPM frame with a total number of time slots ($M = 8$) and signal time slots ($n = 3$). $\Delta\phi$ is the phase difference between any two successive DPSK symbols (signal slots). The performances of these hybrid modulation schemes were evaluated under an optical amplifier noise limit, specifically amplified spontaneous emission (ASE) noise [5]. However, in long-haul optical transmission, the nonlinearity impact becomes a significant limit of the overall system performance [6]. Several approaches have been proposed for modeling the effect of fiber nonlinearity [7–12]. One of these approaches for addressing the nonlinear impacts in SMFs is the Gaussian noise (GN) model. Such a four-wave-mixing (FWM)-based approach models the nonlinear interference as an additive GN that is statistically independent from both the amplifier noise and the transmitted signal [13]. The validation of this approach has been assured over a wide range of system scenarios [9].

In this paper, we adopt the GN model to address the effect of fiber nonlinearity on the performance of hybrid DPSK-MPPM systems. An analytical expression for the total noise variance is obtained for the DPSK-MPPM technique in a nonlinear-dispersive optical channel. Both BER and symbol-error rate (SER) expressions are developed to include the effect of fiber nonlinearity on the performance of DPSK-MPPM systems. Numerical evaluations are then carried out based on the proposed setup supplemented by a realistic simulation scenario for the DPSK-MPPM schemes. The results are compared to that of traditional differential binary PSK (DBPSK), differential quadrature PSK (DQPSK), and MPPM schemes. Furthermore, we discuss the effects of some WDM parameters on optimal system performance. Finally, the nonlinear interference penalties on the maximum reachable distances by both hybrid and traditional modulation systems are investigated at a forward-error-correction (FEC) requirement (BER $= 10^{-3}$).

The rest of the paper is organized as follows. In Section 2, the GN-model specifications are highlighted. We also formulate an expression for the total nonlinear variance of the long-haul DPSK-MPPM optical transmission system. In addition, we develop expressions that consider fiber nonlinearity impacts of the SERs and BERs for DPSK-MPPM systems. In Section 3, we elaborate on the proposed DPSK-MPPM setup and the adopted simulation scenario of the long-haul transmission system. Section 4 is devoted to the performance evaluation and comparison of both hybrid and traditional systems in long-haul transmission. Finally, the conclusion is given in Section 5.

## 2. NONLINEAR MODEL OF DPSK-MPPM SYSTEM

The effect of fiber nonlinearity in long-haul optical transmission is addressed by the GN model [12–14]. Based on the model assumptions, the nonlinear frequency interaction is statistically independent from both the transmitted signal and other system noise [14]. In this model, the total system noise variance can be expressed as

$$\sigma^2 = \sigma_n^2 + \sigma_{\text{nl}}^2, \tag{1}$$

where $\sigma_n^2$ is the complex optical amplifier noise variance, and $\sigma_{\text{nl}}^2$ is the nonlinear interference variance of the complex transmitted signal. In the case of erbium-doped fiber amplifiers (EDFAs), we have $\sigma_n^2 \approx (G-1)Fh\nu B_n$, where $G$ is the amplifier gain, $F$ is the amplifier noise factor, $h$ is Plank's constant, $\nu$ is the center channel frequency, and $B_n$ is the noise bandwidth [11,12,15]. Based on the GN model, the complex transmitted signal should be spectrally sliced as a wavelength-division multiplexed (WDM) signal with $N_{\text{ch}}$ channels, where the WDM is used in the computational model in order to apply the FWM approach. In other words, $N_{\text{ch}}$ of DPSK-MPPM transmitted signals are WDM at the transmitter. Then, a long-haul nonlinear-dispersive SMF is used as the transmission channel. The channel is composed of $N_s$ spans; each span is followed by an EDFA. At the receiver side, the $N_{\text{ch}}$ modulated signals are wavelength-division demultiplexed and processed by separate DPSK-MPPM demodulators, as shown in Fig. 2.

### A. Nonlinear Interference Variance

The nonlinear interference variance $\sigma_{\text{nl}}^2$ is obtained from the nonlinear power spectral density (PSD) of a single-span system at a specific frequency $f$ and distance $z$ [7]

$$S_{\text{nl}}(f,z) = 2\left(\frac{8}{27}\right)^{\delta_{2p}}\gamma^2\int_{-\infty}^{\infty}\int_{-\infty}^{\infty}(H(f_1+f_2-f) \times H(f_2)H(f_1))^2\left|\frac{1-e^{-(2\alpha-j4\pi|\beta_2|f_1f_2)z}}{2\alpha-j4\pi|\beta_2|f_1f_2}\right|^2 \mathrm{d}f_1\mathrm{d}f_2, \tag{2}$$

where $\delta_{2p}$ is the Kronecker delta function with $p = 1$ or $p = 2$ for single polarized- or dual polarized-multiplexed transmission, respectively. $\beta_2$ is the group-velocity dispersion (GVD), $\alpha$ is the attenuation coefficient for SMF, and $\gamma = 2\pi n_2/\lambda A_{\text{eff}}$ is the fiber nonlinearity coefficient, where $A_{\text{eff}}$ is the core effective area, $\lambda$ is the propagated wavelength, and $n_2$ is the nonlinear-index coefficient. $f_1$, $f_2$, and $f_1 + f_2 - f$ are the pump frequencies of the FWM process that create

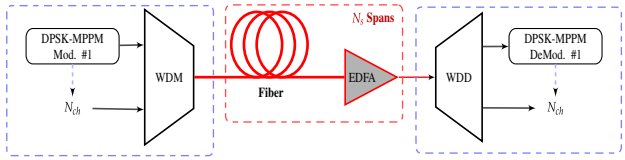


**Fig. 2.** Block diagram of a hybrid DPSK-MPPM long-haul optical transmission; $N_{\text{ch}}$, number of transmitted DPSK-MPPM signals; $N_s$, number of spans; WDM, wavelength-division multiplexer; EDFA, erbium-doped fiber amplifier; WDD, wavelength-division demultiplexer; Mod, modulator; DeMod, demodulator.

the nonlinear interference signal at a frequency $f$. $H(f)$ is the transmitted filtered signal shape, which is assumed to be flat as $H(f) = \sqrt{(MP_{\text{tx}})/(nB_{\text{ch}})}\text{rect}[f/(2B_{\text{ch}})]$, where $P_{\text{tx}}$ is the average launch power, $B_{\text{ch}}$ is the channel bandwidth, which is equal to the sampling rate $R_s$ at the Nyquist limit, and $\text{rect}[f/(2B_{\text{ch}})]$ is the rectangular function with a window width of $2B_{\text{ch}}$.

We obtain a closed-form formula for the nonlinear interference variance $\sigma_{\text{nl}}^2$ by following a similar procedure as [14]. However, we use the approximation of the spectral bands into a square integration area with side length of $\sqrt{3}B_\omega/4$, where $B_\omega = B_{\text{ch}}N_{\text{ch}}$ is the total WDM bandwidth with $N_{\text{ch}}$ channels. This spectral approximation is verified to give a closer result to the exact integral evaluation [16]. In addition, the introduction of the $M/n$ ratio results from replacing the signal peak power by the $P_{\text{peak}} = (MP_{\text{tx}}/n)$ in $H(f)$ expression. Using the identities in [17], an analytical expression for the nonlinear interference variance is obtained by integrating its PSD of Eq. (2) over the noise bandwidth $B_n$:

$$\sigma_{\text{nl}}^2 = \left(\frac{8}{27}\right)^{\delta_{2p}} \frac{\gamma^2}{\pi|\beta_2|}\frac{L_{\text{eff}}^2}{L_{\text{eff,a}}}\left(\frac{MP_{\text{tx}}}{nB_{\text{ch}}}\right)^3 B_n N_s \times \text{arcsinh}\left(\frac{3}{8}\pi^2 L_{\text{eff,a}}|\beta_2|B_\omega^2\right), \tag{3}$$

where $L_{\text{eff}} = (1 - e^{-2\alpha L_s})/2\alpha$ and $L_{\text{eff,a}} = 1/2\alpha$ are the effective and asymptomatic-effective lengths, respectively, for a fiber with a physical span length $L_s$ and an attenuation coefficient $\alpha$. By comparing Eq. (3) to [14], the ratio $M/n$ explicitly appears in order to differentiate between different MPPM levels. In addition, a reduction in the argument of (arcsinh) by 3/4 appears due to the spectral band approximation.

### B. SER of MPPM Systems under Nonlinear Effect

An expression of $\text{SER}_{\text{MPPM}}$ can be obtained using a similar argument as in [5,18,19] but take into consideration that both nonlinearity and ASE noise affect the signal slots, i.e., the total noise variance is $\sigma^2 = \sigma_n^2 + \sigma_{\text{nl}}^2$. However, nonsignal slots are only affected by the ASE noise with variance $\sigma_n^2$.

Assume that the received power per slot has a threshold value of $P_{\text{min}}$ (minimum received power in signal slots). In addition, assume that $r$ out of $n$ received signal slots have this minimum power value, while the rest of the $n - r$ signal slots have power values higher than $P_{\text{min}}$. In this case, the symbol error arises when $s$ nonsignal slots have a power value that reaches $P_{\text{min}}$ or above, while the rest of the $M - n - s$ nonsignal slots have power values below $P_{\text{min}}$. Here, $s$ denotes the number of nonsignal slots with power values $\geq P_{\text{min}}$. Therefore, the symbol error can be upper bounded [5] as

$$\text{SER}_{\text{MPPM}} = \sum_{s}^{M-n}\sum_{r}^{n}\int_0^\infty \binom{n}{r}\binom{M-n}{s}[1-\mathcal{P}_1(\zeta)]^{n-r} \times \left\{\left[1-\mathcal{P}_0\left(\frac{\sigma^2}{\sigma_n^2}\zeta\right)\right]^s + \left[p_0\left(\frac{\sigma^2}{\sigma_n^2}\zeta\right)\right]^s\left[1-\frac{1}{\binom{s+r}{r}}\right]\right\} \times \left[\mathcal{P}_0\left(\frac{\sigma^2}{\sigma_n^2}\zeta\right)\right]^{M-n-s}[p_1(\zeta)]^r d\zeta, \tag{4}$$

where $\zeta = 2B_nP_{\text{min}}/B_{\text{ch}}\sigma^2$, $p_1(\cdot)$ refers to the probability-density function (pdf) of the power in a signal slot, which follows a noncentral chi-squared $\chi^2$ distribution with a noncentrality parameter equal to the peak power, and $p_0(\cdot)$ refers to the pdf of the power in a nonsignal slot, which follows a $\chi^2$ distribution. In addition, $\mathcal{P}_0(\cdot)$ and $\mathcal{P}_1(\cdot)$ are the cumulative distributions corresponding to $p_0(\cdot)$ and $\mathcal{P}_1(\cdot)$, respectively.

### C. BER of DPSK-MPPM Systems Under Nonlinear Effect

An upper bound on the BER of DPSK-MPPM techniques is expressed at any $q$-DPSK modulation level as [5]

$$\text{BER} \leq \frac{1}{N+qn}\left\{\text{SER}_{\text{MPPM}}\left[\frac{N2^N}{2(2^N-1)} + \frac{qn}{2}\right] + q(1-\text{SER}_{\text{MPPM}})\left[\left(\frac{1}{2} - \text{BER}_{\text{DPSK}}\right) \times \text{SER}_{\text{MPPM}} + n\text{BER}_{\text{DPSK}}\right]\right\}, \tag{5}$$

where $\text{SER}_{\text{MPPM}}$ is the symbol-error rate of MPPM data bits, and $\text{BER}_{\text{DPSK}}$ is the bit-error rate of DBPSK or DQPSK data bits on top of the current MPPM frame. Also, $(N + qn)$ denotes the total number of transmitted bits per frame, where $N = \lfloor \log_2\binom{M}{n} \rfloor$ is the number of bits encoded using an MPPM scheme, while $q$ is the DPSK modulation level, i.e., $q = 1$ for DBPSK and $q = 2$ for DQPSK.

BER expressions for both DBPSK and DQPSK [20] can be extended in order to take the nonlinearity impacts as follows:

$$\text{BER}_{\text{DBPSK}} = \left(\frac{1}{2} + \frac{MB_nP_{\text{tx}}}{8nB_{\text{ch}}\sigma^2}\delta_{2p}\right)\exp\left(-\frac{MB_nP_{\text{tx}}}{nB_{\text{ch}}\sigma^2}\right), \tag{6}$$

$$\text{BER}_{\text{DQPSK}} = Q(\varepsilon_+, \varepsilon_-) + \frac{1}{2}\exp\left(-\frac{\varepsilon_+^2 + \varepsilon_-^2}{2}\right) \times \left[\frac{(\varepsilon_+^2 - \varepsilon_-^2)I_1(\varepsilon_+\varepsilon_-)}{4\varepsilon_+\varepsilon_-}\delta_{2p} - I_0(\varepsilon_+\varepsilon_-)\right], \tag{7}$$

where $\varepsilon_\pm = \sqrt{\frac{MB_nP_{\text{tx}}(1\pm\sqrt{1/2})}{nB_{\text{ch}}\sigma^2}}$, $I_r(\cdot)$ is the $r^{\text{th}}$ order modified Bessel function of the first kind, and $Q(\cdot,\cdot)$ is the Marcum $Q$ function.

It is worth mentioning that we assume a perfectly synchronized DPSK-MPPM receiver system. However, the synchronization error (if it exists) can be classified into two types of timing errors. The first is the frame timing error that results due to a timing offset equal to multiple time-slot durations ($m\tau$:$m = 1, \ldots, M-1$). In this case, the DPSK detection will be error-free regardless of the time-offset value because the relative phase difference between any two successive signal slots is not affected by this type of timing error (even if these consecutive signal slots belong to different frames). The second is the time-slot timing error on the time-slot level. This timing error results due to timing offset value $\Lambda\tau$ where $|\Lambda| \leq 0.5$. This is equivalent to what was discussed in [21,22] regarding the timing error of DPSK modulation schemes. The same analysis can be applied in our case such that the $\text{BER}_{\text{DPSK}}$ expression is multiplied by an error factor $\mathfrak{D}(\Lambda)$ as in Eq. (18) in [21]. Here, we assume a perfect synchronized system (i.e., timing-error-free

system). Therefore, in our analysis, the error factor is equal to unity ($\mathfrak{D}(\Lambda) = 1$). On the other hand, there are errors in the MPPM detection process due to these two types of timing errors, as was discussed in [23,24].

## 3. PROPOSED SETUP AND SIMULATION SCENARIO

In this section, the interior structure of the proposed setup and the steps of the simulation scenario are detailed. Our main motivations here are to prove the feasibility of the DPSK-MPPM modulation scheme using the current state of technology and to enhance the precision of the numerical results by adopting a specific setup structure with a particular simulation scenario.

### A. Transmitter Side

The proposed transmitter scheme is depicted in Fig. 3. A coherent laser source emits single-mode light pulses at a rate $1/T$, with each pulse having a period $n\tau$. The pulsed laser emission has a coherence time longer than $2T$, thereby allowing phase information to be reserved along two sequential pulses. A straightforward approach to implement this coherent pulsed laser source is to act on the emission of a coherent continuous-wave diode laser by a fast optical switch. A subsequent traditional DPSK modulator encodes $qn$ phase bits per pulse.

The $qn$ bits modulated light pulse is fed to the MPPM modulator, which consists of a $K$-stages ultra-fast discrete delay line capable of applying up to $2^K$ discrete delay steps [5], where $L$ is the shortest length of polarization-maintaining single-mode (PMSM) fiber per delay stages. This discrete delay line modulates the position of each phase-modulated time-slot pulse into one of $M$ locations, where the number of available slot positions per frame $M \leq 2^K$. The synchronized electro-optic polarization switching within the delay line precisely chops the phase-modulated pulse into $n$ pulses. Both DPSK and MPPM modulators are controlled via the transmitter signal-processing unit (T-SPU), which is synchronized to the pulsed laser source, thereby carrying out the precise timing required by the hybrid DPSK-MPPM modulation. The input data of T-SPU is thus $\lfloor \log_2 \binom{M}{n} \rfloor + qn$ bits. While DPSK data is forwarded by the T-SPU directly to the DPSK modulator, the MPPM data is manipulated first by the T-SPU to produce the $K$ delay controls. In addition, a subsequent control is used to unify the polarization of the delay output regardless of the introduced delay. It should be mentioned that, based on the current state of technology, the proposed DPSK-MPPM system is capable of manipulating high data rates up to 50 Gbit/s [5,25,26].

The simulation scenario is described in Fig. 4. A pseudo random binary sequence (PRBS) is used for generating the transmitted data with lengths of $\lfloor \log_2 \binom{M}{n} \rfloor + qn$ bits. These data bits are split into two parts. The first $N = \lfloor \log_2 \binom{M}{n} \rfloor$ bits are encoded using the MPPM scheme. Each MPPM signal slot is then DPSK-modulated using additional $q$ bits. The optical fiber is simulated as a nonlinear-dispersive channel, i.e., a complex additive GN is added to the transmitted signal. Both nonlinear interference and ASE noise sources (i.e., $\sigma^2 = \sigma_n^2 + \sigma_{\text{nl}}^2$) are added to the signal slots, whereas only ASE noise $\sigma_n^2$ is added to the nonsignal slots.

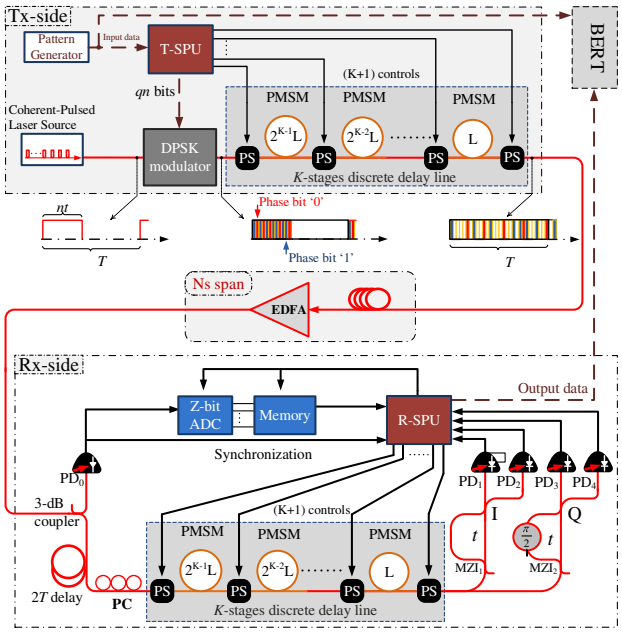


**Fig. 3.** Proposed setup of hybrid DPSK-MPPM long-haul system; T-SPU (R-SPU), transmitter- (receiver)-signal processing unit; PS, polarization switch; PD, photodetector; ADC, analog-to-digital converter; PC, polarization controller; PMSM, polarization maintaining single-mode fiber; DDL, discrete delay line; BERT, BER tester; MZI, Mach–Zehnder interferometer.

### B. Receiver Side

At the receiver side, the received signal is split into two distinct arms, MPPM and DPSK receivers, as shown in Fig. 3. In order

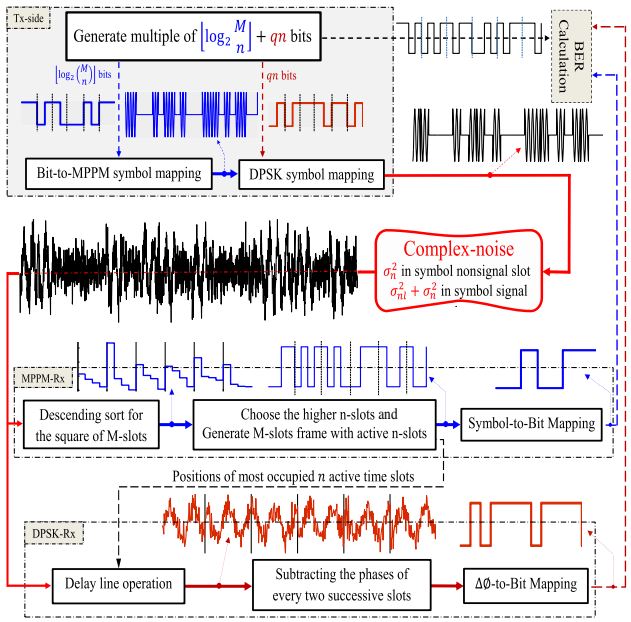


**Fig. 4.** Simulation scenario of a hybrid DPSK-MPPM technique long-haul system with signal flow depicted at different stages of the simulation scenario. A DBPSK-MPPM signal case study of ($M = 4$ and $n = 2$) is used.

to decode the phase information, the positions of the active $n$ slots should be defined first. A photodetector on the MPPM (upper) arm listens to the optical intensity along the frame period and feeds a subsequent Z-bits analog-to-digital converter (ADC). The ADC and its memory storage are triggered by the edge of time-slot clock generated by the receiver signal-processing unit (R-SPU). This clock is precisely synchronized to the transmitter's pulses by transmitting a periodic reference frame. The memory storage records the signal intensity within each time slot whether occupied or not. The R-SPU runs a comparison routine on the $M$ stored values, resulting in a soft decision regarding the position of the most occupied $n$ time slots. On the DPSK arm, a two-frame delay holds the processing of the phase information until the best decision regarding the active $n$ time-slot positions is made by the R-SPU. The R-SPU, being aware of the positions of the time slots, can adapt the receiver delay line to act by the complementary delay made by the transmitter for each signal slot, thereby reallocating them in contiguous time slots.

The phase encoded signal is then split between two Mach–Zehnder interferometers (MZIs) whose unbalanced arms differ precisely by the time-slot period $\tau$, while one of them involves $\pi/2$ phase shift between its two arms. Although only one MZI is sufficient for DBPSK decoding, two MZIs are needed to run the phase compensation process, as will be discussed later. The R-SPU eventually encapsulates the DPSK bits along with the MPPM bits, recovering back the sent frame data.

It is worth noticing that a receiver equipped with a $K$-stages discrete delay line matched to that at the transmitter will certainly suffer a different delay-induced phase pattern (an ideally matched delay line, however, can perfectly compensate for the delay-induced phase). In order to compensate this phase perturbation, the transmitter and receiver run an initial reconciliation routine as follows. The transmitter sends a training sequence, which has supposedly no phase information. This frame has $M$ contiguous signal slots with the first slot traversing the fastest path along the PMSM fiber of all stages, while each following signal slot trains one of the delay steps in order. This training sequence is thus chopped owing to the different delay of each signal slot while conveying solely the phase accumulated by the delay line of the transmitter for each delay possibility. The R-SPU acts using the receiver delay line on each frame slot by a delay value complementary to that of the transmitter, thereby recombining the signal slots. Then, using the two MZIs in the I and Q arms, the receiver measures the relative phase accumulated (due to the delay lines of the transmitter and receiver) within each slot compared with the preceding one. The R-SPU then stores the absolute phase value corresponding to each delay step to be able to compensate for the delay-induced phase.

It should be noted that the received DPSK-MPPM signal in the simulation scenario in Fig. 4 is processed as in the proposed setup. The simulation scenario can be explained as follows: the received signal is fed into both the DPSK and MPPM receiver branches. In the MPPM branch, the positions of the most occupied $n$ time slots from the $M$ time-slots frame are determined through a descending-order operation. Using the positions of the most occupied $n$ time slots, the received frame is generated by setting ones in the indicated $n$ slots and zero in the remaining $M - n$ slots. Then, a MPPM symbol-to-bit decoding is performed to produce the detected MPPM data bits. In the DPSK branch, by using the positions of the most occupied $n$ time slots (active slots) that are fed from the MPPM branch, the active $n$ time slots (that contain the DPSK phase information) are reallocated in contiguous time slots. The aforementioned operation performs the same function as the delay line in the proposed setup. Then, the relative phase shifts $\Delta\phi$ between the consecutive active time slots are estimated. This relative phase shifts are DPSK-decoded into data bits through $\Delta\phi$-to-bit mapping. Finally, the BER will be estimated by comparing the received data bits with the transmitted ones.

## 4. NUMERICAL RESULTS

Here we numerically study the performance of DPSK-MPPM modulation techniques in long-haul transmission. We assume a standard SMF with $\alpha = 0.22$ dB/km, $D = 16.7$ ps/km · nm, and $\gamma = 1.3$ W$^{-1}$ km$^{-1}$. An EDFA with gain $G = e^{2\alpha L_s}$ compensates the fiber span loss, and the noise figure is 6 dB. The WDM specifications are: $B_{\text{ch}} = R_S = 32$ GHz and $B_n = 12.48$ GHz [0.1 nm is the reference resolution for optical signal-to-noise ratio (OSNR) calculation]. The total fiber length is 1000 km with a 100 km span length [14]. It should be mentioned that the quantization error of the ADC is ignored in our numerical evaluation.

Figure 5 shows the BERs versus average launch optical power per channel for different single-polarized single-channel hybrid DPSK-MPPM systems using both analytical expression and Monte Carlo simulation based on the schematic scenario in Fig. 4. The bits-to-symbol mapping and demapping of MPPM ($M = 4$ and $n = 2$) and ($M = 8$ and $n = 3$) are carried out as in [27]. According to the proposed setup in Fig. 3, these arrangements require a discrete delay line with $K \geq \log_2 M$, that is, $K \geq 2$ or 3 for $M = 4$ or 8, respectively. It can be noticed that for different DPSK-MPPM systems, the theoretical results are very tight to the simulation results, which justifies that our upper-bound BER is very close to the exact BER

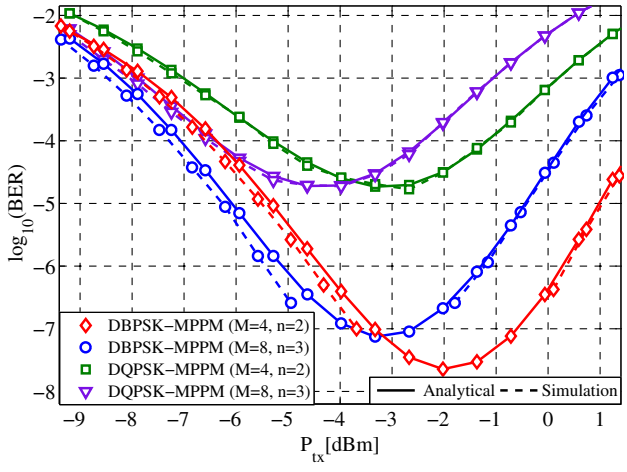


**Fig. 5.** BER versus average launch optical power per channel for both hybrid DBPSK-MPPM and DQPSK-MPPM systems; analytical and simulation results are shown with solid and dashed curves, respectively. The system has $N_s = 20$ with 100 km span length.

expressions. The hybrid system's performance is enhanced by increasing the launch power in the linear region. This linear region is extended to the optimal-average launch power (at which the minimum BER occurs). In the linear region, two performance limits can occur: the first one results from the ASE noise only and is called the linear limit, and the second limit results from both the nonlinearity and ASE noise under the condition that the ASE noise is still dominant that is called the low-nonlinearity limit. On the other hand, in the nonlinear region, where the power level is greater than the optimal-average launch power, the effect of the nonlinearity becomes dominant. In the nonlinear region, an increase in the launch optical power results in a degradation of the hybrid system performance. It should be noticed that the optimal performance is achieved at an average launch power [15]

$$P_{\text{opt.}} = 1.5^{\delta_{2p}} \frac{n}{M} \sqrt[3]{\frac{\pi L_{\text{eff,a}} |\beta_2| B_{\text{ch}}^3 (G-1) F h\nu}{2\gamma^2 L_{\text{eff}}^2 \operatorname{arcsinh}(\frac{3}{8}\pi^2 L_{\text{eff,a}} |\beta_2| B_\omega^2)}}. \quad (8)$$

This optimal-average launch power is directly proportional to the active $n$ time slots and inversely proportional to the number of time slots per frame $M$. Indeed, it can be seen from Fig. 5 that as the $M/n$ ratio increases, the optimal performance occurs at lower average power values.

Figures 6 and 7 depict the BERs versus average launch optical power per channel for single-channel hybrid DBPSK-MPPM systems compared with corresponding MPPM and DBPSK systems, respectively, for dual polarized-multiplexed transmission. Both $M$ and $n$ are chosen so as to ensure that all systems under comparison have the same transmission data rate. In the linear region, the hybrid system performance is improved by increasing $M$ as the energy efficiency of the system is improved. Specifically, from Fig. 6 at BER $= 10^{-3}$ (FEC-requirement), there is a power savings of about 2.5 dB for the hybrid DBPSK-MPPM system ($M = 16$ and $n = 3$) when compared to the traditional MPPM system ($M = 16$ and $n = 5$). Moreover, it can be seen from Fig. 7 that the hybrid system ($M = 22$ and $n = 6$) provides a power savings of about 0.5 dB when compared to traditional DBPSK. The last power savings increases to about 1 dB at BER $= 10^{-4}$. The reason behind this improvement is that when transmitting same data rate and bandwidth at a specific average optical power, hybrid systems have higher peak power per slot as compared to corresponding traditional MPPM and DBPSK systems. This leads to a higher SNR and improved BER. Furthermore, if we take into account the nonlinearity effect in the linear region (low-nonlinearity limit), the hybrid DPSK-MPPM system still outperforms the traditional ones. In addition, the savings in the average launch optical power in the hybrid system is the same as mentioned above.

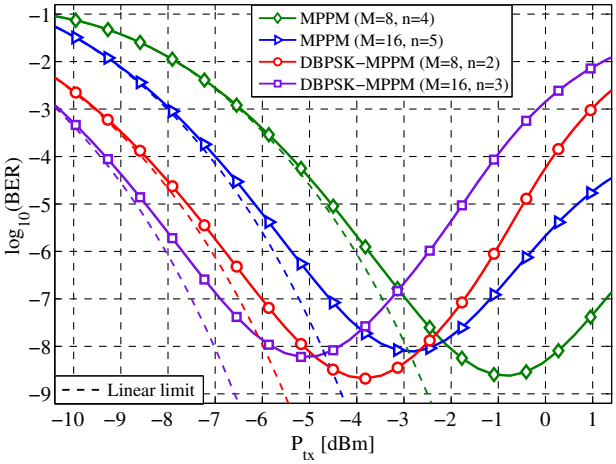


**Fig. 6.** BER versus average launch optical power per channel for both hybrid DBPSK-MPPM and traditional MPPM systems, including the linear limited case (dashed curves).

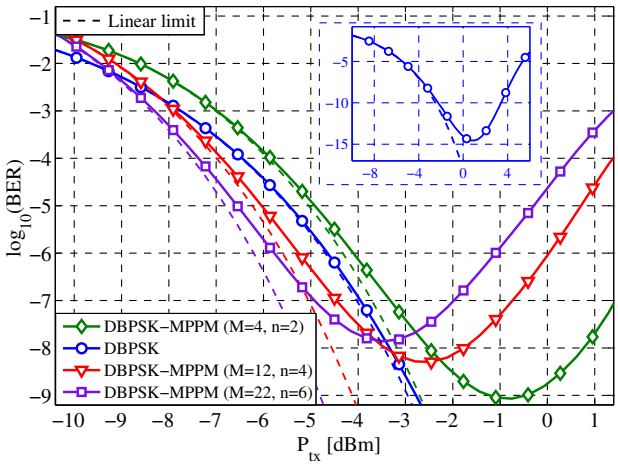


**Fig. 7.** BER versus average launch optical power per channel for both hybrid DBPSK-MPPM and traditional DBPSK systems, including the linear limited case (dashed curves). The inset shows a traditional DBPSK system.

After a specific peak power corresponding to the optimal-average launch power, the nonlinearity impact becomes dominant over the ASE noise effect. Because of the proportionality of the nonlinear noise variance to $P_{\text{peak}}^3 = (MP_{\text{tx}}/n)^3$, the overall SNR of the hybrid systems is reduced when compared to the traditional systems because the hybrid systems have higher peak power per slot under the transmission of the same data rate and bandwidth. Therefore, the hybrid DBPSK-MPPM system is affected more rapidly by fiber nonlinearity than traditional DBPSK and MPPM systems.

The effect of changing the $(M, n)$ level can be discussed as follows: in the linear region, by increasing the ratio $M/n$, the performance of both MPPM and DPSK-MPPM systems is improved. The reason behind this improvement is the enhancement of the energy efficiency of the MPPM-based systems by increasing the ratio $M/n$. However, in the nonlinear region, the effect is reversed; the higher the $M/n$ ratio, the higher the fiber nonlinear interference that results in a performance degradation. This increase in the fiber nonlinear interference is due to the increase of the peak power per slot by increasing the ratio $M/n$. Furthermore, it is should be observed that an increase in the $M/n$ ratio results in degradation of the optimal BER performance, as shown form various curves in both Figs. 6 and 7.

It is worth observing that at very small average launch power, traditional DBPSK achieves better performance than that of the hybrid system (Fig. 7) because, in the case of very

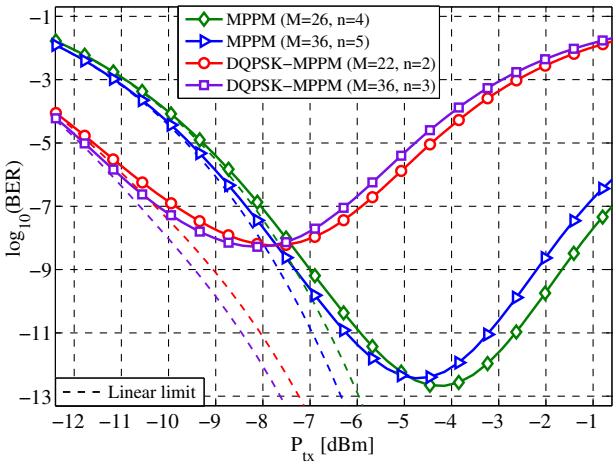


**Fig. 8.** BER versus average launch optical power per channel for both hybrid DQPSK-MPPM and traditional MPPM systems, including the linear limited case (dashed curves).

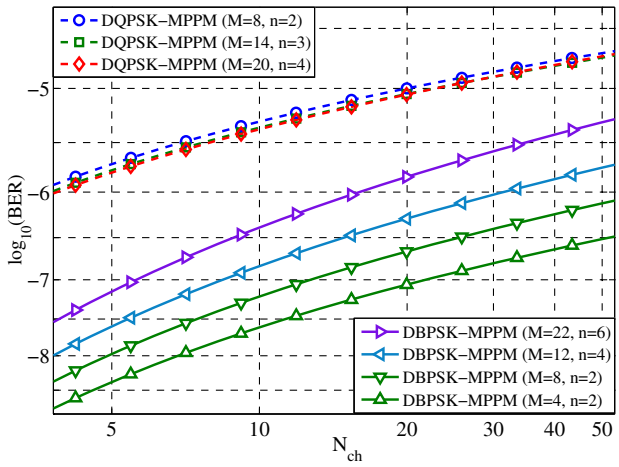


**Fig. 10.** Optimal BER versus number of WDM channels for different hybrid DBPSK- and DQPSK-MPPM systems. The WDM channel bandwidth is $B_{ch} = 32$ GHz.

low launch power, the ASE noise has a dominant effect over the high peak power per slot benefit of the hybrid system. This leads to an increase in $SER_{MPPM}$, as it depends on the relative power difference between received signal and noise. However, the $BER_{DBPSK}$ symbols do not depend on the received signal power, but rather on the phase difference between the constitutive received bits, which results in a much higher noise margin for DBPSK system than MPPM techniques.

The aforementioned conclusions for the hybrid DBPSK-MPPM system apply for the single-channel hybrid DQPSK-MPPM system as well. Specifically, from Fig. 8 at BER $= 10^{-3}$ (FEC requirement), there is a power savings of about 2.5 dB for the hybrid DQPSK-MPPM system ($M = 36$ and $n = 3$) when compared to a traditional MPPM system ($M = 36$ and $n = 5$). Furthermore, it can be seen from Fig. 9 that the hybrid system ($M = 20$ and $n = 4$) provides a power savings of about 2 dB when compared to the traditional DBPSK.

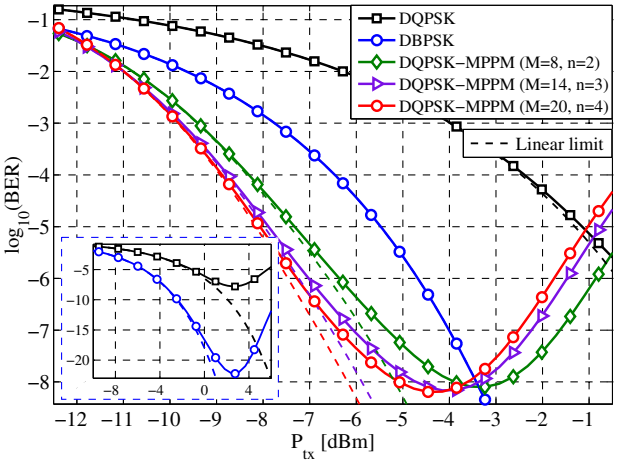


**Fig. 9.** BER versus average launch optical power per channel for both hybrid DQPSK-MPPM and traditional DBPSK and DQPSK systems, including the linear limited case (dashed curves). The inset shows traditional DBPSK and DQPSK systems.

In addition, after considering the low-nonlinearity effect, the last improvements do not change. It is worth mentioning that the relative performance trend is unchanged whatever the value of the M/n ratio, as shown from different curves with various $M/n$ ratios in Figs. 6–9.

Next, we study the effect of WDM characteristics on the performance of the hybrid DPSK-MPPM/WDM system. In Figs. 10 and 11, we show the effect of both the number of WDM channels and the channel bandwidth, respectively, on the optimal performance of the hybrid DPSK-MPPM systems. It can be noticed that the optimal system performance is degraded by increasing the number of WDM channels or channel bandwidth. The reason for that degradation can be analytically explained due to the inverse proportionality between the SNR and both the number of WDM channels and the channel bandwidth. Furthermore, it can be physically interpreted as an increase in the number of WDM channels increases the inter-channel nonlinear interaction, and an increase in the

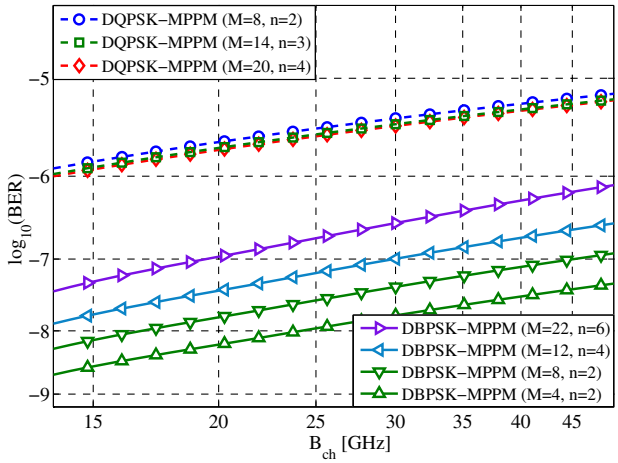


**Fig. 11.** Optimal BER versus WDM channel bandwidth for different hybrid DBPSK- and DQPSK-MPPM systems. The WDM system has $N_{ch} = 9$.

WDM channel bandwidth increases the per-channel nonlinear interference power. This leads to an increase in the overall nonlinearity impact, thus the optimal performance of the DPSK-MPPM system will be degraded. Moreover, we can notice that an increase in the ratio $M/n$ for the hybrid DBPSK-MPPM results in a degradation in the optimal system performance under a specific transmission data rate. This is not due to the decrease in the value of the SNR, which does not depend on the $M/n$ ratio at optimal performance. Rather, increasing the ratio $M/n$ will increase the $\mathrm{SER}_{\mathrm{MPPM}}$ and as a result the performance is degraded. However, for the hybrid DQPSK-MPPM, the performance is almost independent of the ratio $M/n$ under the same transmission data rate. The reason behind that can be explained as follows. At optimal performance, the $\mathrm{BER}_{\mathrm{DQPSK}}$ dominates over the $\mathrm{SER}_{\mathrm{MPPM}}$ and cancels the effect of the increase in the $\mathrm{SER}_{\mathrm{MPPM}}$ while increasing the ratio $M/n$. In addition, the optimal performance depends on the differential phase modulation level. It can be noticed that the optimal performance of the DBPSK-MPPM system is better than that of the DQPSK-MPPM one at the same $M = 8$ and $n = 2$ because DQPSK has doubled the transmission data rate of DBPSK at a specific bandwidth that leads to an increase of the error probability in the DQPSK system compared with that of the DBPSK system. Thus, a higher performance degradation for DQPSK-MPPM is found compared with DBPSK-MPPM at the same $M/n$ ratio.

Figure 12 shows the nonlinear penalty on the maximum distance that can be reached by the hybrid and the traditional modulation systems at a BER of $10^{-3}$ (FEC requirement). As mentioned earlier, the hybrid modulation systems are more sensitive to fiber nonlinearity than traditional DPSK and MPPM systems. At low launch power, under the same transmission rate and channel bandwidth, the maximum reach of the hybrid systems is better than that of traditional ones. Specifically, at an average transmitted power of −10 dBm, the DQPSK-MPPM system with ($M = 36$ and $n = 3$) reaches a distance more than that of the MPPM system with ($M = 36$ and $n = 5$) by about 570 km. Moreover, at an average transmitted power of −8 dBm, the maximum reach of the DQPSK-MPPM system with ($M = 20$ and $n = 4$) is longer than that of traditional DQPSK and DBPSK by about 1000 km and 345 km, respectively, and the maximum reach of the DBPSK-MPPM with ($M = 16$ and $n = 3$) is longer than that of the traditional MPPM system with ($M = 16$ and $n = 5$) by about 600 km. On the other hand, by increasing the launch power, the nonlinear interference becomes more significant. Therefore, the hybrid modulation systems lose their high sensitivity benefit, and their maximum reach becomes worse than that of traditional ones, which is clear from Fig. 12. It is worth mentioning that, under the same transmission rate and channel bandwidth, the maximum reach of the hybrid systems increases by increasing the ratio $M/n$. However, by increasing the launch power, the hybrid system's maximum reach is decreased by increasing the ratio $M/n$ as the nonlinear interference becomes more significant.

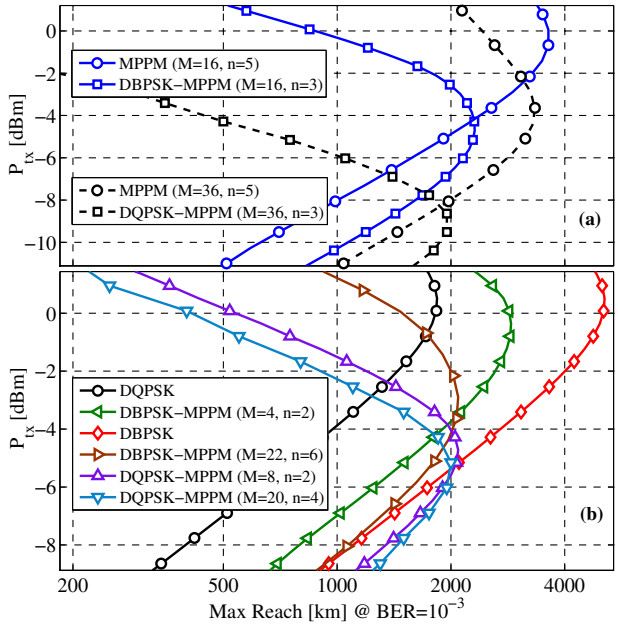


**Fig. 12.** Optical launch power versus maximum achievable reach at BER $= 10^{-3}$ (FEC requirement) for different DPSK-MPPM systems compared to corresponding traditional (a) DPSK and (b) MPPM systems. The WDM system has $N_{\mathrm{ch}} = 9$ and $B_{\mathrm{ch}} = 32$ GHz.

## 5. CONCLUSIONS

The effects of optical fiber nonlinearity on hybrid DPSK-MPPM techniques have been studied in long-haul nonlinear-dispersive optical transmission using the GN model. Closed-form expressions for the nonlinear interference variance of DPSK-MPPM for both single and dual polarized systems have been derived along with corresponding upper bounds of BERs. The tightness of the BER's upper bounds has been verified using Monte Carlo simulation. We have run the numerical analysis in light of a proposed setup, which represents a design viewpoint for the DPSK-MPPM system. The performance of the hybrid DPSK-MPPM technique has then been compared to that of traditional DBPSK, DQPSK, and MPPM techniques. Our results reveal that the DPSK-MPPM technique is less robust against fiber nonlinearity than traditional techniques. However, it outperforms them in both linear and low-nonlinearity limits. Finally, the performance evaluation has been extended to include WDM system characteristics. Our results reveal that the hybrid system's optimal performance is degraded by increasing the number of WDM channels, channel spacing, $M/n$ ratio (in case of DBPSK-MPPM system only), or differential phase modulation level. Furthermore, at the FEC requirement, under the same transmission rate and channel bandwidth, the maximum reach of the hybrid systems has been shown to be better than that of traditional ones at low launch power; however, the situation is reversed at high launch power. Therefore, the hybrid modulation systems are more suitable in low power transmission cases.

**Funding.** Egyptian Ministry of Higher Education (MoHE); National Telecom Regulatory Authority (NTRA), Egypt.

## REFERENCES

1. R. Essiambre and R. Tkach, "Capacity trends and limits of optical communication networks," Proc. IEEE **100**, 1035–1055 (2012).

2. X. Liu, S. Chandrasekhar, T. H. Wood, R. W. Tkach, P. J. Winzer, E. C. Burrows, and A. R. Chraplyvy, "M-ary pulse-position modulation and frequency-shift keying with additional polarization/phase modulation for high-sensitivity optical transmission," Opt. Express **19**, B868–B881 (2011).
3. X. Liu, T. H. Wood, R. W. Tkach, and S. Chandrasekhar, "Demonstration of record sensitivities in optically preamplified receivers by combining PDM-QPSK and M-Ary pulse-position modulation," J. Lightwave Technol. **30**, 406–413 (2012).
4. M. Sjödin, T. A. Eriksson, P. A. Andrekson, and M. Karlsson, "Long-haul transmission of PM-2PPM-QPSK at 42.8 Gbit/s," in *Optical Fiber Communication Conference and Exposition and the National Fiber Optic Engineers Conference (OFC/NFOEC)* (2013), pp. 1–3.
5. A. E. Morra, H. M. H. Shalaby, S. F. Hegazy, and S. S. A. Obayya, "Hybrid direct-detection differential phase shift keying-multipulse pulse position modulation techniques for optical communication systems," Opt. Commun. **357**, 86–94 (2015).
6. P. P. Mitra and J. B. Stark, "Nonlinear limits to the information capacity of optical fibre communications," Nature **411**, 1027–1030 (2001).
7. A. Carena, V. Curri, G. Bosco, P. Poggiolini, and F. Forghieri, "Modeling of the impact of nonlinear propagation effects in uncompensated optical coherent transmission links," J. Lightwave Technol. **30**, 1524–1539 (2012).
8. P. Serena, A. Bononi, and N. Rossi, "The impact of the modulation dependent nonlinear interference missed by the Gaussian noise model," in *European Conference on Optical Communication (ECOC)* (2014), pp. 1–3.
9. A. Nespola, S. Straullu, A. Carena, G. Bosco, R. Cigliutti, V. Curri, P. Poggiolini, M. Hirano, Y. Yamamoto, T. Sasaki, J. Bauwelinck, K. Verheyen, and F. Forghieri, "GN-model validation over seven fiber types in uncompensated PM-16QAM Nyquist-WDM links," IEEE Photon. Technol. Lett. **26**, 206–209 (2014).
10. K. Peddanarappagari and M. Brandt-Pearce, "Volterra series transfer function of single-mode fibers," J. Lightwave Technol. **15**, 2232–2241 (1997).
11. W. Shieh and X. Chen, "Information spectral efficiency and launch power density limits due to fiber nonlinearity for coherent optical OFDM systems," IEEE Photon. J. **3**, 158–173 (2011).
12. P. Poggiolini, G. Bosco, A. Carena, V. Curri, Y. Jiang, and F. Forghieri, "A detailed analytical derivation of the GN model of non-linear interference in coherent optical transmission systems," arXiv:1209.0394 [physics] (2012).
13. H. Louchet, A. Hodzic, and K. Petermann, "Analytical model for the performance evaluation of DWDM transmission systems," IEEE Photon. Technol. Lett. **15**, 1219–1221 (2003).
14. P. Poggiolini, G. Bosco, A. Carena, V. Curri, Y. Jiang, and F. Forghieri, "The GN-model of fiber non-linear propagation and its applications," J. Lightwave Technol. **32**, 694–721 (2014).
15. G. Bosco, P. Poggiolini, A. Carena, V. Curri, and F. Forghieri, "Analytical results on channel capacity in uncompensated optical links with coherent detection," Opt. Express **20**, 19610–19611 (2012).
16. S. Savory, "Approximations for the nonlinear self-channel interference of channels with rectangular spectra," IEEE Photon. Technol. Lett. **25**, 961–964 (2013).
17. A. Jeffrey and D. Zwillinger, *Table of Integrals, Series, and Products*, 7th ed. (Academic, 2007).
18. J. Hamkins and B. Moision, "Multipulse pulse-position modulation on discrete memoryless channels," Interplanetary Netw. Progr. Rep. **42**, 1–13 (2005).
19. A. E. Morra, H. S. Khallaf, H. M. H. Shalaby, and Z. Kawasaki, "Performance analysis of both shot- and thermal-noise limited multipulse PPM receivers in gamma–gamma atmospheric channels," J. Lightwave Technol. **31**, 3142–3150 (2013).
20. K.-P. Ho, *Phase-Modulated Optical Communication Systems* (Springer, 2005).
21. M. K. Simon, "A simple evaluation of DPSK error probability performance in the presence of bit timing error," IEEE Trans. Commun. **42**, 263–267 (1994).
22. K. Kiasaleh and T. He, "On the performance of DQPSK communication systems impaired by timing error, mixer imbalance, and frequency nonselective slow Rayleigh fading," IEEE Trans. Veh. Technol. **46**, 642–652 (1997).
23. K. Sato, T. Ohtsuki, I. Sasase, and S. Mori, "Performance analysis of (m, 2) MPPM with imperfect slot synchronization," in *IEEE Pacific Rim Conference on Communications, Computers and Signal Processing* (1993), pp. 765–768.
24. K. Sato, T. Ohtsuki, and I. Sasase, "Coding for multi-pulse PPM with imperfect slot synchronization in optical direct-detection channels," IEICE Trans. Commun. **E78-B**, 916–922 (1995).
25. "Polarization modulators," Versawave Technologies, 2014, https://versawave.com/products/polarization-modulators/.
26. S. Koeber, R. Palmer, M. Lauermann, W. Heni, D. L. Elder, D. Korn, M. Woessner, L. Alloatti, S. Koenig, P. C. Schindler, H. Yu, W. Bogaerts, L. R. Dalton, W. Freude, J. Leuthold, and C. Koos, "Femtojoule electro-optic modulation using a silicon–organic hybrid device," Light Sci. Appl. **4**, e255 (2015).
27. F. Xu, M. Khalighi, and S. Bourennane, "Coded PPM and multipulse PPM and iterative detection for free-space optical links," J. Opt. Commun. Netw. **1**, 404–415 (2009).